Parallel calibration transfer and systematic effects in retrospective absorbed dose estimation using OSL

C.I. Burbidge[1, 3], J. Cardoso[2], G.O. Cardoso[1], J. Franco[1], L. Santos[2], M. Caldeira[2]

[1]C[2]TN, Instituto Superior Técnico, Universidade de Lisboa. Portugal.
[2]LPSR, Instituto Superior Técnico, Universidade de Lisboa. Portugal.
[3]GeoBioTec, Universidade de Aveiro, Portugal
christoph@ctn.ist.utl.pt

Abstract

Parallel multiple aliquot calibration transfer is combined with evaluation of standardized single aliquot regenerative OSL dose response characteristics to produce a robust and efficient transfer protocol for mineral samples used in dating and retrospective dosimetry. This is implemented from an IST-LPSR ^{60}Co primary air kerma standard, to a matrix of quartz-based sample types (activated, heated, bleached) plus polymineral in different Risø and Daybreak ^{90}Sr/^{90}Y irradiators, on different support types (aluminium 0.5 mm; stainless steel 0.25 and 0.5 mm), of different grain sizes (90/100-160 μm; 160-250 μm), for different signal integrals (Ch11-30, 391-490; Ch11-13, 14-15). Differences between grainsize and support ranged up to 25% but were specific to the irradiator-support-grainsize permutation, e.g. for the oldest Risø irradiator, source-sample distance and backscatter compensate for the smaller grainsize, but this is not the case in more recent models or for larger grains, while in the Daybreak this is not compensated so differences depend straightforwardly on support material. Calibration transfer results are compared with retrospective absorbed dose evaluation using SAR-OSL. Measured/given beta exposures were close to unity for activated and heated material, which exhibited predose sensitization, and vice versa for optically bleached samples. Each value was best reproduced for gamma irradiation when using the respective multiple aliquot calibration coefficient. Parallel multiple aliquot calibration transfer using OSL integrated over the majority of signal decay was found to offer better accuracy and precision than retrospective single aliquot measurements, and was robust for polyminerals as well as quartz.

Keywords: Calibration; OSL; Quartz/Polymineral; SAR dose recovery; Precision; Accuracy

1. Introduction

TSL/OSL dosimetry systems are routinely based on parallel calibration using a photon source, with beta irradiations limited to use for dose-normalisation (Alves et al., 2006; Ambrosi et al., 2000; Piesch 1981). However, for reduced shielding requirements and convenience in applications where repeated exposure and measurement of a single sample is advantageous, such as luminescence dating and retrospective dosimetry, beta sources are often used for both dose-normalisation and reference irradiation (Bortolot and Bluszcz, 2003; Markey et al., 1997; Oberhofer, 1981; Richter et al., 2012; Sanderson and Chambers, 1985). Beta source geometry, scatter from the source matrix and shielding, backscatter from the dosemeter support, and attenuation in the dosemeter, make it desirable that dosimetric calibration transfer from a standard photon source is established for each specific permutation of beta irradiator, dosemeter type, and dosemeter support to be used.

Calibration transfer for the luminescence response of materials measured in dating and retrospective dosimetry is subject to non-linear dose response, inhomogeneous sensitivity to radiation, dependence on pretreatment and measurement conditions, and signal instability. If the transfer protocol involves retrospective evaluation of the given photon dose, then the calibration is also specific not only to the sample/irradiator geometry, but also to the dosemeter preparation and measurement protocol. Parallel preparation, multiple aliquot gamma and beta irradiation, and measurement, permits elimination of many systematic effects (Bassinet et al., 2006; Pernicka and Wagner, 1979; Piesch, 1981). Parallel procedures are relatively intensive in labour and sample quantity: the retrospective application of multiple aliquot, and in recent decades particularly single aliquot, procedures (with careful sample pretreatment) has gained favour as being efficient and precise (Bassinet et al., 2014; Bos et al 2006; Correcher and Delgado, 1998; Göksu et al., 1995; Goedicke 2007; Mauz and Lang, 2004; Richter, 2003). This advantage has been applied for the evaluation of multiple grainsizes and support types (Armitage and Bailey, 2005; Goedicke 2007; Mauz and Lang, 2004). Potential systematic effects in retrospective quartz single aliquot OSL procedures have been described by Stokes (1994) and Murray and Wintle (2000). Some aspects relating to their correction were investigated by Bailey (2000) and Singhvi et al. (2012). Use of the properties of ‘standardised’ dose response characteristics, i.e. dose-normalised signal multiplied by normalisation dose, can help characterise differences in the form of dose response and deal efficiently with non-linearity effects (Burbidge et al., 2006; Burbidge, 2015; Roberts and Duller, 2004).

Retrospective measurement of previously gamma or beta irradiated quartz, based on an existing calibration transfer, has been used to test the relative severity of systematic effects between different measurement conditions, protocols, or samples (Ballarini et al., 2007; Bassinet et al., 2006; Burbidge et al., 2006; Burbidge et al., 2011; Kadereit and Kreutzer, 2013; Murray and

Wintle, 2003; Roberts et al., 1999; Thomsen et al., 2005). This yields ratios of given to measured or estimated dose, and has been termed "dose recovery" (Murray and Wintle, 2003). In some studies, efforts have been made to adjust measurement conditions to yield measured to given ratios of unity (Kadereit and Kreutzer, 2013), and differences have been observed between gamma and beta irradiation (Thomsen et al., 2005). It is impossible to verify that "dose recovery" in the laboratory is the same as that for dating or retrospective dosimetry using the same sample, due to different exposure and storage conditions (Bassinet et al., 2006; Burbidge, 2003; Burbidge et al., 2010). The same problem applies to retrospective calibration transfer using previously gamma irradiated material, so that it becomes important to understand potential systematic effects on the transfer (Kadereit and Kreutzer, 2013). Understanding gained under controlled conditions may then be applicable to the blind measurement of samples for retrospective dosimetry and dating.

Parallel calibration transfer using quartz has recently been investigated by Guérin and Valladas (2014). They compared parallel retrospective absorbed dose evaluations from gamma and beta irradiated aliquots, for optically bleached grains from sedimentary quartz and heated grains from quartzite. With the exception of Göksu et al. (1995), Richter et al. (2003), Pernicka and Wagner (1979), the aforementioned calibration transfer studies have all used the same type of beta irradiator (Risø), although of different generations with Sr/Y elements of foil and different configurations of ceramic. Calibration transfer for two of the irradiators used in the present study was previously established for 100 μm quartz on stainless steel cups and fine grains on aluminium disks by Richter et al. (2003).

The present work has the objectives of generating and comparing parallel and retrospective calibration transfer for activated, heated and optically bleached quartz (and polymineral) samples, taking into account common supports and grainsize for three generations of Risø irradiator and a Daybreak irradiator of similar but different design. The overall aim is to unite robust traditional parallel calibration transfer with modern approaches to luminescence measurement and absorbed dose evaluation in a single internally consistent protocol.

2. Materials and Methods

2.1. Experimental design

Seven samples were selected for analysis, having a variety of archaeological and geological histories (Table 1), and OSL behaviours (Table 5). Mineral grains were prepared from each sample and pretreated in bulk to reset the luminescence signal (Table 1). Groups of aliquots were prepared on different types of support, these were irradiated using beta sources and

retained as blanks, in parallel with gamma irradiation of a separate subsample of quartz in a fused silica box (Fig. 1; Table 2). Aliquots were then prepared from the gamma irradiated grains. A delay was allowed to render any differences in irradiation time insignificant, and then all aliquots were measured in parallel using a SAR-OSL protocol: one reader per type of sample support (Fig. 1; Table 4). Calibration coefficients (sβ per $Gy^{60}Co$) were obtained by comparing standardised signals between aliquots (i.e. multiple aliquot), and compared with the results of single aliquot 'dose recovery' values.

2.2. Sample preparation

Quartz grains were prepared from six of the samples by sieving in either of two grainsize fractions (90 or 100 - 160 μm, and 160 – 250 μm), washing in HCl (10%, 10 min) then H_2O_2 (10%, 10 min), density separation in polytungstate solution (2.62-2.7 g cm^{-3}), treatment with HF (40%, 40 min) then HCl (10%, 10 min), then reseived wet at 90/100 or 160 μm. Resultant material was checked under an optical microscope and by a combined initial luminescence test measurement (Rodrigues et al., 2013): density separation and/or HF treatment plus wet reseive were repeated to minimise the presence of other minerals and smaller grainsizes. Polimineral grains were prepared from a seventh sample by sieving and washing in HCL. Prepared material from sample A12/175 was annealed, irradiated, and heated, to sensitize luminescence signals (Martini et al., 1984; Toyoda et al., 1996). That from the remaining samples was pretreated in a manner expected to be similar but less severe than the archaeological or geological resetting event they had been subject to (350 °C; or daylight filtered by window glass for 1 - 4 weeks; Table 1).

2.3. Beta and Gamma Irradiations

For beta irradiation and OSL measurement, mineral grains were mounted as monolayers on the central portions of three different types of support (stainless steel cups, aluminium disks, and stainless steel disks; Table 2), using Silkospray silicone oil with 5 mm mask. Beta irradiations of each sample on each type of support were performed in four different models of irradiator, with differing source and sample presentation geometries (Fig. 1; Table 2; irradiation times $t_{\beta 1}$ (s) are listed in Table 5).

Gamma irradiations were conducted using an encapsulated ^{60}Co source mounted in an Eldorado 6 irradiator (Table 2), in a low-scatter geometry for which an ion-chamber based primary standard air kerma calibration is established by LMRI, IST (Allisy-Roberts et al., 2009; Cardoso et al., 2007a, b) and maintained to an accuracy of ±0.44% at 95% confidence. Quartz grains

were irradiated inside a rectangular cuboid fused silica box (Table 2), in two steps, with the box facing in opposite directions. Bulk density of the fused silica box was measured using Archemedes principle, that of the quartz powders assumed (Table 2). Mass-thicknesses of the wall and edge-to-centre of the sample were 0.81 and 0.64 gcm^{-2}. Total exposures were adjusted to 5 Gy air kerma in air at the sample location: exposure times ranged from 48 to 56 minutes through the period of the study. Conversion of air kerma to absorbed dose in quartz was evaluated using montecarlo calculations in MCNP5 (Brown et al., 2010) and EGSnrc (Kawrakow, 2000), and analytically from standard reference data, to provide a basic means of cross-checking the performance of each approach and understanding the contribution of different components to the final result.

The analytical treatment was as follows:

$$\frac{D_S}{K_{ColA}}(\text{sample centre}) = \frac{\mu_{enQ}}{\mu_{enA}} B_{W+S/2} e^{-\mu_{totQ}\left(\rho_W t_W + \rho_S t_S/2\right)}$$

$$\frac{D_S}{K_{ColA}}(\text{sample/wall interface}) = \frac{\mu_{enQ}}{2\mu_{enA}} \left\{ B_W e^{-\mu_{totQ}\rho_W t_W} + B_{W+S} e^{-\mu_{totQ}(\rho_W t_W + \rho_S t_S)} \right\} \quad (1)$$

$$B \simeq \begin{cases} 1 + (b-1)\dfrac{K^{\mu_{nc}\rho t} - 1}{K - 1}, & K \neq 1 \\ 1 + (b-1)\mu_{nc}\rho t, & K = 1 \end{cases}$$

$$K = c(\mu_{nc}\rho t)^a + d\,\frac{\tanh\left(\dfrac{\mu_{nc}\rho t}{\xi} - 2\right) - \tanh(-2)}{1 - \tanh(-2)}$$

Where K_{ColA} = collisional air kerma (Gy), D_S = absorbed dose in the quartz sample (Gy), μ_{tot} = total mass attenuation coefficient (cm^{2}g^{-1}), μ_{nc} = mass attenuation coefficient neglecting coherent scattering (cm^{2}g^{-1}), μ_{en} = mass energy absorption coefficient (cm^{2}g^{-1}), ρ = bulk density (gcm^3), t = thickness (cm), W = wall, S = sample (i.e. detector volume), A = air, B = photon scattering buildup factor, K a b c d and ξ are paramenters in the geometric progression (G-P) approximation (Table 3).

Attenuation and buildup of K_{ColA} was approximated assuming a broad beam of 1.25 MeV photons normally incident on planes of fused silica and quartz grains. These mass thicknesses are 2 and 1.5 times the extrapolated range for maximum Compton electron energy (E_γ = 1.25 MeV, T_{emax} = 1.04 MeV, $R_{\text{cdsa}}(T_{emax})$ = 0.52 gcm^{-2}, $R_{\text{ext,t}}(T_{emax})$ = 0.41 gcm^{-2}; Krane 1988 Ch 7; ICRU 1984; Tabata et al., 2002; Fig. 2), so transient cpe with respect to the external

environment is established in the wall, and the detector (sample) is large relative to secondary electron ranges. Mass attenuation coefficients were obtained directly from XCOM (Berger et al., 2010). Energy absorption coefficients and exposure geometric progression (G-P) buildup parameters for 1.25 MeV photons were interpolated from Trubry (1988, tables 2 and 3; Table 3), directly for air and using Z_{eq} of 10.72 calculated for SiO_2 (Harima, 1983 in Sharaf et al., 2015). Although kerma from the primary photons is attenuated 5.5% at entry to the sample (from the front wall) and 11.3% at exit from the sample (to the rear wall), the buildup of kerma from secondary photons largely compensates in this geometry, giving 1.2% and 2.8% overall reductions respectively. In addition to averaging the effects of attenuation and buildup, underestimate of D by K_{Col} in conditions of transient cpe is largely compensated by reversing the direction of the sample halfway through irradiation. After accounting for the difference in μ_{en} between air and quartz, D_S/K_{ColA} in the sample at the wall/sample interface and in its centre are both estimated to be 0.9785. The overall effect of varying wall thickness by ±0.1 mm or varying sample bulk density between 1.5 and 1.7 g cm^{-3}, both produced systematic deviation in D_S/K_{ColA} of less than 0.0005. However, scatter in of additional electrons from the walls is expected to add to this, since the bulk density of the wall is 1.375 times that of the sample. An analytical treatment of scatter-in (Fig. 2) indicates up to ca. 3.5% higher transported energy adjacent to the walls and an overall increase of D_S/K_{ColA} (assuming all the extra transported energy is deposited in the sample) of 0.5% to 0.9832.

Calculations in EGSnrc were made using the predefined user code DOSRZnrc (Kawrakow, 2000). A ^{60}Co spectrum from a collimated encapsulated source was presented at air 20 cm in front of the box containing the quartz sample, in a 5 cm radius beam from a point source at 60 cm. Sample/box/air geometry was approximated as concentric end-on cylinders of r (cm) = 0.4/0.77/5, l (cm) = 0.8/1.52/32. The circumference/cross-sectional area and surface-area/volume of this simulated sample cylinder is equal to that of the actual cuboid. For comparison with the analytical estimate a planar approximation was also made, with r (cm) = 0.4/5/5. Photons were forced to interact at least once in the sample/box/air volume. Profiles of K_{ColS} (colisional kerma from primary and scattered photons in the quartz sample) and D_S were obtained for 0.4 cm radius, 0.036 cm thick slices along the source-sample axis, and K_{ColA} registered in the same volumes following substitution of sample and wall for air (Fig. 3). Distortion of K_{ColS} and D_S vs. depth due to scatter-in, was not evident for the contrast in bulk densities used in the present work. K_{ColS} and D_S scores for volume elements at equal distances from the front and rear face of the box were averaged to account for reversal of the box halfway through irradiation. Dose and kerma quotients were calculated based on the mean ($\pm 1\sigma/n^{1/2}$) of these values for the 20 volume elements comprising the sample (SiO_2 of bulk density 1.6 g cm^{-3}). D_S/K_{ColA} for the planar approximation was 0.9915(±0.0006, 10^8 emitted photons), 0.8%

higher than estimated analytically. 10^9 particle histories per run in the cylindrical approximation gave D_S/K_{ColA} = 0.9690(±0.0028), K_{ColS}/K_{ColA} = 0.9705(±0.0028).

Calculations in MCNP5 (Allisy-Roberts et al., 2009; Cardoso et al., 2007a, b) implemented the cuboid box and sample, and the full irradiation geometry (Table 2), assuming an effective point source emitting a ^{60}Co photon spectrum. K_{ColS} was calculated for the entire sample volume using the *f6 tally. K_{ColA} was calculated for the same volume after replacing sample and box with air. 10^8 particle histories per run gave K_{ColS}/K_{ColA} = 0.9770±0.0018 at 1σ, and so D_S/K_{ColA} = 0.976. The difference between D_S/K_{ColA} estimated using EGSnrc and MCNP was 0.7%, and yet significantly larger than the statistical errors associated with each calculation. To allow for this, the working value adopted for air kerma to sample dose conversion was 0.9725(±0.0035).

2.4. Luminescence Measurements

Three of the beta sources in the calibration transfer were integrated in Risø automatic TL/OSL readers, equipped with U340 detection filters: each reader was used to measure all aliquots on one type of sample support (SSC, ALD, SSD; Fig. 1; Table 4), using a SAR protocol with preheat 240°C/30s, test preheat 160°C/30s. OSL was measured at 125°C and IRSL at 50°C, both for 125 s at 60% power. Two different sets of OSL signal integrals were used: channels 11-30 minus background channels 391-490 ("late background subtraction") to measure the majority of the OSL signal, and channels 11-12 minus background channels 13-14 to measure the initial gradient of OSL decay. This "late" and "early" background subtraction have been found to produce different results in luminescence dating studies (Ballarini et al., 2007). Signal resulting from the parallel beta, gamma, and blank irradiation was thus the first signal measured, I_1 (cts), in the SAR sequences (Table 4). Standardized signal, I_{S1} (sβ), was calculated using I_1 and the first test dose response in the SAR sequence (Table 4; Table 5; Roberts and Duller, 2004):

$$I_{S1} = t_{\beta T} . I_1 / I_{T1}$$

Single aliquot estimates of beta exposure time were made using the SAR-OSL response measured from each aliquot, by interpolating I_{S1} through single saturating exponential fits to I_S from the remaining SAR cycles, $t_{\beta SAR}$ (s), (Murray and Wintle, 2000; Roberts and Duller, 2004). Outlying results were rejected. For certain aliquots, multiple layers of grains were observed in coincidence with differences in $t_{\beta SAR}$ between background subtraction methods. Accepted results were used to calculate weighted means (1/var) of $t_{\beta SAR}$ for each group of aliquots (R1, R2, R3,

Db, ^{60}Co, Bl; SSC, ALD, SSD; Fig. 1; Table 5). Uncertainty at 1σ was estimated as the larger of the internal and external error values (Burbidge et al., 2006; Thomsen et al., 2005).

"Single aliquot" beta dose rates (2) were calculated from the values of beta exposure time obtained from gamma irradiation and SAR measurement of the gamma irradiated aliquots ($t_{\beta\,^{60}Co,SAR^{60}Co}$), minus the values of beta exposure time obtained from blank irradiation and SAR measurement of the blank irradiated aliquots ($t_{\beta Bl,SARBl}$):

$$\dot{D}_{\beta SA}\left(mGy^{60}Co.s^{-1}\right)=\frac{D_{^{60}Co}}{\left(t_{\beta\,^{60}Co,SAR^{60}Co}-t_{\beta Bl,SARBl}\right)} \quad (2)$$

For the "multiple aliquot" evaluation of dose rates (3), weighted means (1/var) of I_{S1} were calculated for each group of aliquots (R1, R2, R3, Db, ^{60}Co, Bl; SSC, ALD, SSD; Fig. 1; Table 5). Uncertainty at 1σ was estimated as the larger of the internal and external error values. Differences in the standardized signal produced by the beta, gamma, and beta test exposures, combined with the saturating exponential form of the dose response characteristic, produce differences in signal per unit dose between I_S obtained from different groups of aliquots (Burbidge et al., 2006). To evaluate this, the weighted mean of I_{S1} for each group was interpolated through a single saturating exponential fit to the weighted means of I_S from the remaining SAR cycles, averaged across all groups, i.e. all aliquots of a given measurement or {sample; support/reader} permutation. This produced values of $t_{\beta\beta,SARall}$ for each beta exposed group, and $t_{\beta\,^{60}Co,SARall}$ for the gamma exposed group. Signal per unit beta exposure time for gamma exposure was calculated as $\left(I_{S1^{60}Co}-I_{S1Bl}\right)/t_{\beta\,^{60}Co,SARall}$, and that for beta exposure as $(I_{S1\beta}-I_{S1Bl})/t_{\beta\beta,SARall}$.

"Multiple aliquot" beta dose rates were calculated for each beta irradiated group, from the quotient of I_S beta minus I_S blank and I_S gamma minus I_S blank, multiplied by the quotient of gamma dose rate and beta exposure time, multiplied by the quotient of signal per unit beta exposure during beta exposure and that during gamma exposure (3).

$$\dot{D}_{\beta MA}\left(mGy^{60}Co.s^{-1}\right)=\frac{\left(I_{S1\beta}-I_{S1Bl}\right)}{\left(I_{S1^{60}Co}-I_{S1Bl}\right)}\frac{D_{^{60}Co}}{t_{\beta 1}}\frac{\frac{\left(I_{S1\beta}-I_{S1Bl}\right)}{t_{\beta\beta,SARall}}}{\frac{\left(I_{S1^{60}Co}-I_{S1Bl}\right)}{t_{\beta\,^{60}Co,SARall}}}=\frac{\left(I_{S1\beta}-I_{S1Bl}\right)^2}{\left(I_{S1^{60}Co}-I_{S1Bl}\right)^2}\frac{t_{\beta\,^{60}Co,SARall}}{t_{\beta\beta,SARall}}\frac{D_{^{60}Co}}{t_{\beta 1}} \quad (3)$$

The beta dose rate values from each sample were corrected for decline in $^{90}Sr/^{90}Y$ activity ($t_{1/2}$ 28.8 years, to 01/01/2014), and weighted means (1/var; external error 1σ) calculated to obtain a calibration coefficient, *C*, for each permutation of beta irradiator, support, grainsize, and OSL signal integral {(R1, R2, R3, Db); (SSC, ALD, SSD); (90/100-160 μm, 160-250 μm); ([11-30 391-490], [11-12 13-14])}. Comparison of the average internal and external errors on *C* for the different OSL signal integrals and approaches to calculating $\dot{D}_{\beta}$, across all combinations of reader, support and grainsize (Table 6), indicated that while single aliquot approaches yielded better precision, dispersion was minimised by using the dose-normalised multiple aliquot approach and the signal integrals 11-30, 391-490. Dose rates from the multiple aliquot data of the polymineral sample A7/318 were within the range observed for quartz, and were included in the weighted means. The resultant calibration coefficients (Table 7) were compared between grain sizes and types of support by taking ratios, to evaluate patterns of variation as a function of backscatter and beta field homogeneity (Table 8; Fig. 4).

The ratio measured/given beta exposure (s/s) was calculated as the weighted mean of $t_{\beta SAR\beta}/t_{\beta 1}$ for the one group of aliquots per sample that had been irradiated and then measured by SAR-OSL on the same reader and hence also the same support (Table 9). For comparison, estimated/given gamma dose (Gy/Gy) was calculated for the same groups as measured/given β exposure, using i. $\dot{D}_{\beta MA}$ obtained from that particular group (3), ii. the weighted mean of $\dot{D}_{\beta SA}$ (2) for a given support and grainsize (i.e. "C_{SA}"), and iii. C_{MA} from Table 7, i.e. the weighted mean of $\dot{D}_{\beta MA}$ (3) for a given support and grainsize:

i. estimated/given gamma dose = $\frac{\dot{D}_{\beta MA} t_{\beta SAR^{60}Co}}{D_{^{60}Co}}$

ii. estimated/given gamma dose = $\frac{C_{SA}\, t_{\beta SAR^{60}Co}{}'}{1000 D_{^{60}Co}}$

iii. estimated/given gamma dose = $\frac{C_{MA}\, t_{\beta SAR^{60}Co}{}'}{1000 D_{^{60}Co}}$

, where $t_{\beta SAR^{60}Co}{}'$ is $t_{\beta SAR^{60}Co}$ corrected for decay of the $^{90}Sr/^{90}Y$ source to 01/01/2014.

3. Results and Discussion

The beta calibration coefficients evaluated for 90/100-160 μm grains on stainless steel cups in R1 and Db were 2.3% and 2.6% higher than decay corrected values for 100 μm grains based on Richter et al. (2003): respectively ca. 1σ and 2σ based on the present uncertainty estimates. Present results are thus considered to be consistent with the previous calibration transfer exercise.

Optimal precision in calibration coefficients was obtained using dose normalised signals integrated over the majority of the OSL decay, with late background subtraction, in a multiple aliquot approach (Table 6). Values obtained using initial OSL signals with early background subtraction were similar: for a given permutation of beta irradiator, grainsize and support, they were within 3.4% and 1.1 times the combined 1σ uncertainty excluding systematic uncertainties in the gamma dose delivered to the quartz (Table 7). The difference may relate simply to poorer counting statistics. Also, in some cases outlying results from individual aliquots appeared (on subsequent inspection) to relate to the presence of multiple layers of grains on the support: in these cases results from initial signals and early background subtraction tended to be less severely affected.

The relatively high dispersion obtained using a single aliquot approach (Table 6) may relate to effects of "dose recovery" on its accuracy (Table 9). For the present experimental conditions, values of measured/given beta exposure ($t_{\beta SAR}/t_{\beta}$, section 2.4) provided direct control on the accuracy of the SAR measurement of the signal from ^{60}Co irradiation. Weighted mean values of $t_{\beta SAR}$ for each sample were up to 21% different from the known exposure time t_{β}. The lowest values were obtained from optically bleached samples, which did not exhibit predose sensitization (Fig. 5). Activated and heated samples yielded values close to unity, and did exhibit predose sensitization (Fig. 5). Use of $\dot{D}_{\beta MA}$ (2) and C_{SA} to calculate estimated/given gamma dose produced values with similar strong sample to sample variation as $t_{\beta SAR}/t_{\beta}$ (Std. Dev. 7-10%), but that were all shifted so that the average was close to unity. Thus, use of $\dot{D}_{\beta MA}$ (2) and C_{SA} tended to correct for the average effects of "beta dose recovery", but would not then permit the use of $t_{\beta SAR}/t_{\beta}$ to accurately correct a measurement of an unknown "dose" for "dose recovery" effects. For C_{MA} on the other hand, estimated/given gamma doses were consistent with measured/given beta exposures (RMSD 3%; i.e. systematic effects of measurement did not affect C_{MA}), so that accurate correction for the effect of "dose recovery" could be made using $t_{\beta SAR}/t_{\beta}$. The recycling ratio, conventionally used to assess change in dose response characteristic within the SAR protocol, reproduced $t_{\beta SAR}/t_{\beta}$ for heated quartz (values close to unity) and for the polymineral sample (A7/318), but it did not reflect low values of $t_{\beta SAR}/t_{\beta}$ in the other cases.

Monitoring of and correction for such effects within regenerative measurement sequences applied to quartz has been investigated by Murray and Wintle (2000) and Sinhvi et al. (2012), and its testing will be reported separately.

The present results indicate differences in calibration coefficient for different combinations of grainsize and support (Table 7; Table 8). This may be understood in terms of electron backscatter (and attenuation), and spatial uniformity of the electron fluence in the plane of the sample, i.e. effective solid angle (Table 2; Fig. 4; Carrillo, 1996; Soum et al., 1987; Spooner and Alsop, 2000; Tabata et al., 1999). Differences between C_{SSD} and C_{ALD}, 25% and 14% for 90/100-160 and 160-250 μm grains respectively, are consistent with greater backscatter from steel in a given geometry, and indicate that the difference affects quartz closer (than 100 μm) to the surface of the support. The value of 14% is similar to that obtained by Mauz and Lang (2004) and Armitage and Bailey (2005) for similar grainsizes. For C_{SSC}, reduced steel thickness and increased distance from the Risø beta source (R1, R2, R3) results in a calibration coeficient similar to C_{ALD} for 90/100-160 μm grains, as intended, but it overcompensates for 160-250 μm grains. The difference in source-sample distance for cups and disks is less in the Daybreak irradiator (Bortolot, pers comm, 2015; Table 2) than in the Risø systems, where there is only a small difference between C_{SSD} and C_{SSD}. 160-250 μm grains received on average 8(±1)% and 5(±3)% lower dose rates than 90/100-160 μm grains on SSC and SSD, but 3(±2)% higher dose rates on ALD (Table 7). Similar results for SSC and SSC also indicate that most of the difference in energy deposition relates to backscatter of electrons incident on the support with $E_0 < 0.5$ MeV (Fig. 4), where the difference in η_{BE} for SSC and SSC is small. The low observed difference in calibration coefficient between two different coarse grainsize fractions for ALD (Table 8) is consistent with previous observations by Armitage and Bailey (2005), and the decrease observed for SSC and SSD is not inconsistent with those of Goedicke (2007) if some of the latter's results for slightly larger grainsizes are considered outliers. The reduction at larger grainsizes observed by Goedicke (2007) may relate to a decreased contribution from backscattered electrons rather than attenuation in the grains *per se*. It should be noted though, that the findings of these studies were both based on single aliquot evaluations of what is termed here $t_{\beta SAR60Co}$ ("gamma dose recovery"), but obtained from different samples in different conditions. Although only two broad grainsizes typical of dating studies were used in the present study, the present multiple aliquot results were consistent across various samples and gamma irradiations, as were the relative differences for different types of support.

In the use of a single dose response characteristic in the evaluation of the signal per unit dose quotient (section 2.4), it is assumed that any change in the standardized dose response characteristic from cycle 1 to the remainder, measured by SAR, is equal for each beta- and

386 gamma- exposed group. The parallel treatment, irradiation and measurement of the groups was
387 designed for this, but this aspect was not monitored. However, when using a single fit for all
388 aliquots of a sample (Fig. 5) the signal per unit dose quotient ranged from 0.97 to 1.00, but use
389 of individual group weight means produced much more highly dispersed values, from 0.89 to
390 1.15. The weighted mean standardised response is lower for the polymineral sample (Fig. 5) due
391 to the effect of preheats (preceeding I and I_T) of different severity on a continuous trap
392 distribution, and for samples measured on cups due to either improved thermal contact
393 compared to disks or stronger heating on the reader R1 (Roberts and Duller, 2004; Burbidge,
394 Accepted). Except for this the standardised dose response was the same for all samples, once the
395 calibrated in Gy. Weighted mean standardized signals from the individual groups values appear
396 to include dispersion in signal per unit dose from effects other than change in the gradient of the
397 dose response characteristic. Where multiple aliquot calibration transfer has been pursued in the
398 past, non-linearity effects have been accounted for by relying on subsequent "dose recovery"
399 measurements (regenerative or additive), or by selecting two or three beta irradiation times for
400 each sample to bracket the expected gamma response and so permit linear interpolation (Guerin
401 and Valhadas, 2014), or by calculating a simple ratio but only after an iterative series of
402 previous calibration excecises (Pernicke and Wagner, 1979). Use of two beta irradiation times
403 would have implied doubling the number of aliquots measured per calibration transfer, or an
404 approximately √2 reduction in statistical precision. However, ideally the I_{S1} multiple aliquot
405 dose response characteristic for the different beta and gamma sources would be reconstructed
406 (Bos et al., 2006; Guérin and Valladas, 2014), with consequent multiplication of experimental
407 effort. The experimental effort involved in such approaches has tended to result in use of a
408 limited number of samples, whereas the present results indicate the importance of repeated
409 cycles comparing different samples.
410
411 **4. Conclusions**
412
413 A robust and efficient parallel multiple aliquot calibration transfer protocol for minerals used in
414 luminescence dating and retrospective dosimetry was implemented using standardized OSL
415 signals, and accounting for non-linearity based on a common (weighted mean) SAR-OSL dose
416 response characteristic. The permutations examined included: activated, heated and optically
417 bleached quartz, and polyminerals; supported on aluminium disks, stainless steel cups, and
418 stainless steel disks; for three generations of Risø and one Daybreak beta irradiator; with results
419 calculated using different OSL signal integration times. Results for the different coarse
420 grainsizes were relatively consistent on aluminium disks, but exhibited consistent differences on
421 steel cups and disks, and the relationship between each grainsize/support permutation varied

consistently between irradiators, as a function of backscatter, presentation geometry, and source model.

For the present samples, SAR-OSL from heated material exhibited predose sensitisation and yielded the measured or measured / given beta dose quotients close to unity. Optically bleached material exhibited little sensitivity change and underestimated given beta doses by on average 15%. Comparison of measured/given beta exposures and estimated/given gamma doses indicated that if a parallel multiple aliquot calibration transfer is conducted, then the ratio of measured to given beta exposure may be used to accurately correct for systematic deviations arising from the applied measurement protocol, with an RMS deviation of ca. 3% from sample to sample. However, if the calibration transfer were based on SAR gamma dose recovery then its accuracy would be subject to the rigorously parallel establishment of measured/given beta exposure values, and so effectively it would need to be made into a multiple aliquot approach. Use of OSL integrated over the majority of the decay with "late background" subtraction offered slightly better precision than use of the initial OSL gradient, but was more sensitive to overloading of disks. Parallel multiple aliquot calibration transfer was found to offer better accuracy and precision than retrospective single aliquot measurements, and was robust for polyminerals as well as quartz.

Acknowledgements

FCT PTDC/AAC-AMB/121375/2010; FCT PEst-OE/CTE/UI4035/2014; FCT UID/Multi/04349/2013.

References

Allisy-Roberts, P.J., Burns, D.T., Kessler, C., Cardoso, J. 2009. Comparison of the standards for air kerma of the ITN (Portugal) and the BIPM for 60Co γ-rays. Metrologia, Volume 46, Issue 1A, pp. 06007

Alves, J.G., Abrantes, J.N., Margo, O., Rangel, S., Santos, L. 2006. Long-term stability of a TLD-based individual monitoring system. Radiat. Prot. Dosim. 120, 289-292.

Ambrosi, P., Fantuzzi, E., de Carvalho, A.F., Delgado, A., Lindborg, L., Bartlett, D.T. 2000. Procedures for routine individual dose assessment of external radiation within EU countries and Switzerland - Status of Harmonisation on 1 April 1999. Radiat. Prot. Dosim. 89, 7-51.

Armitage, S.J., Bailey, R.M. 2005. The measured dependence of laboratory beta dose rates on sample grain size. Radiat. Meas. 39, 123-127.

459 Bailey, R.M. 2000. Circumventing possible inaccuracies of the single aliquot regeneration
460 method for the optical dating of quartz. Radiat. Meas. 32, 833-840.
461 Ballarini, M., Wallinga, J., Wintle, A.G., Bos, A.J.J. 2007. A modified SAR protocol for optical
462 dating of individual grains from young quartz samples. Radiat. Meas. 42, 360-369.
463 Bassinet, C., Woda, C., Bortolin, C., Della Monaca, S., Fattibene, P., Quattrini, M.C., Bulanek,
464 B., Ekendahl, D., Burbidge, C.I., Cauwels, V., Kouroukla, E., Geber-Bergstrand, T.,
465 Piaskowski, A., Marczewska, B., Bilski, P., Sholom, S., McKeever, S., Smith, R.,
466 Veronese, I., Galli, A., Panzeri, L., Martini, M. 2014. Retrospective radiation dosimetry
467 using OSL on electronic components: results of an inter-laboratory comparison. Radiat.
468 Meas. 71, 475-479.
469 Bassinet, C., Mercier, N., Miallier, D., Pilleyre, T., Sanzelle, S., Valladas, H. 2006.
470 Thermoluminescence of heated quartz grains: Intercomparisons between SAR and
471 multiple-aliquot additive dose techniques. Radiat. Meas. 41, 803-808.
472 Berger, M.J., Hubbell, J.H., Seltzer, S.M., Chang, J., Coursey, J.S., Sukumar, R., Zucker, D.S.,
473 and Olsen, K. (2010), XCOM: Photon Cross Section Database (version 1.5). [Online]
474 Available: http://physics.nist.gov/xcom. National Institute of Standards and
475 Technology, Gaithersburg, MD.
476 Bortolot, V.J., Bluszcz, A. 2003. Strategies for flexibility in luminescence dating: procedure-
477 oriented measurement and hardware modularity. Radiat. Meas. 37, 551–555.
478 Bos, A.J.J., Wallinga, J., Johns, C., Abellon, R.D., Brouwer, J.C., Schaart, D.R., Murray, A.S.
479 2006. Accurate calibration of a laboratory beta particle dose rate for dating purposes.
480 Radiat. Meas. 41, 1020-1025.
481 Brown, F., Kiedrowski, B., Bull, J. 2010. "MCNP5-1.60 Release Notes", LA-UR-10-06235
482 Burbidge, C.I. 2003. Luminescence investigations and dating of anthropogenic palaeosols from
483 South Mainland Shetland, Unpublished PhD Thesis, University of Wales, Aberystwyth.
484 396 p.
485 Burbidge, C.I. 2015. A broadly applicable function for describing luminescence dose response.
486 Journal of Applied Physics. 118, 044904; doi: 10.1063/1.4927214
487 Burbidge, C.I., Duller, G.A.T., Roberts, H.M. 2006. De determination for young samples using
488 the standardized OSL response of coarse grain quartz. Radiat. Meas. 41, 278-288.
489 Burbidge, C.I., Rodrigues, A.L., Dias, M.I., Prudêncio, M.I., Cardoso, G.O. 2010. Optimisation
490 of preparation and measurement protocols for luminescence dating of small samples
491 from a suite of porcelains and faiences. Mediterranean Archaeology and Archaeometry
492 10, 53-60.
493 Burbidge, C.I., Cabo Verde, S.I., Fernandes, A.C., Prudêncio, M.I., Botelho, M.L., Dias, M.I.,
494 Cardoso, G. 2011. Dosimetry in the multi kilo-Gray range using optically-stimulated

luminescence (OSL) and thermally-transferred OSL from quartz, Radiat. Meas. 46, 860-865.

Cardoso, J., Santos, L., Oliveira, C. 2007a. Air Kerma Primary Standard: Experimental and Simulation Studies on Cs-137. Workshop on "Absorbed Dose and Air Kerma Primary Standards. LNE, CEA-LIST-LNHB & BIPM - 9-11 may, 2007, Paris.

Cardoso, J., Carvalho, A.F., Oliveira, C. 2007b. Simulation studies on a prototype ionization chamber for measurement of personal dose equivalent, HP(10). Radiation Protection Dosimetry 125, 175–179

Carrillo, H.R.V. 1996. Geometrical efficiency for a parallel disk source and detector. Nucl. Instr. Meth. Phys. Res. A 371, 535-537.

Correcher, V., Delgado, A. 1998. On the use of natural quartz as a transfer dosimeter in retrospective dosimetry. Radiat. Meas. 29, 411-414.

Goedicke, C. 2007. Calibration of a $^{90}Sr/^{90}Y$-source for luminescence dating using OSL. Radiat. Meas. 42, 1427-1431.

Göksu, H.Y., Bailiff, I.K., Bøtter-Jensen, L., Brodski, L., Hütt, Y.G., Stoneham, D. 1995. Interlaboratory beta source calibration using TL and OSL on natural quartz. Radiat. Meas. 24 479-483.

Guérin, G., Valladas, H. 2014. Cross-calibration between beta and gamma sources using quartz OSL: Consequences of the use of the SAR protocol in optical dating. Radiat. Meas. 68, 31-37.

Harima, Y. 1983. An approximation of gamma-ray buildup factors by modified geometric progression. Nucl. Sci. Eng. 83, 299–309.

ICRU 1984. International Commission on Radiation Units and Measurements. ICRU Report 37, Stopping Powers for Electrons and Positrons.

Kadereit, A., Kreutzer, S., 2013. Risø calibration quartz - A challenge for β-source calibration. An applied study with relevance for luminescence dating. Measurement 46, 2238-2250.

Kawrakow., I. 2000. Accurate condensed history Monte Carlo simulation of electron transport. I. EGSnrc, the new EGS4 version. Medical Physics 27, 485-98.

Krane, S.K. 1988. Introductory Nuclear Physics. Wiley.

Lapp, T. and Thomsen, K.J. 2010. Beta source uniformity in the Risø TL/OSL reader. UK TL/OSL/ESR meeting, Oxford, 8-10 September 2010. Book of abstracts pp 42.

Markey, B.G., Bøtter-Jensen, L., Duller G.A.T. (1997). A new flexible system for measuring thermally and optically stimulated luminescence. Radiation Measurements 27, 83-89.

Martini, M., Sibilia, E., Spinolo G., Vedda, A. 1984. Ionic conductivity and thermoluminescence in β–irradiated quartz. In Induced defects in insulators P. Mazzoldi (ed.) June 5th - 8th, 1984, Strasbourg, France. 59-64.

Mauz, B., Lang, A., 2004. The dose rate of beta sources for optical dating applications: a comparison between fine silt and fine sand quartz. Ancient TL 22, 45-48.

Murray, A.S., Wintle, A.G. 2000. Luminescence dating of quartz using an improved single-aliquot regenerative-dose protocol. Radiat. Meas. 32, 57-73.

Murray, A.S., Wintle, A.G. 2003. The single aliquot regenerative dose protocol: potential for improvements in reliability. Radiat. Meas. 37, 377-381.

Oberhofer, H. 1981. Ch 4 Accessory instrumentation. In Applied Thermoluminescence Dosimetry. Eds M Oberhofer and A Scharmann. Ch 11, ECSC, EEC, EAEC, Brussels and Luxembourg, 67-80.

Pernicka, E., Wagner, G.A. 1979. Primary and interlaboratory calibration of beta sources using quartz as thermoluminescent phosphor, Ancient TL 6, 2–6.

Piesch, E. 1981. Application of TLD systems for environmental monitoring. In Applied Thermoluminescence Dosimetry. Eds M Oberhofer and A Scharmann. Ch 11, . ECSC, EEC, EAEC, Brussels and Luxembourg, 197-228.

Richter, D., Zink, A., Przegietka, K., Cardoso, G.O., Gouveia, M.A., Prudêncio, M.I. 2003. Source calibrations and blind test results from the new Luminescence Dating Laboratory at the Instituto Tecnológico e Nuclear, Sacavém, Portugal. Ancient TL 21, 1-7.

Richter, D., Pintaske, R., Dornich, K., Krbetscheck, M. 2012. A novel beta source design for uniform irradiation in dosimetric applications. Ancient TL 30, 57-64.

Rodrigues, A.L., Burbidge, C.I., Dias, M.I., Rocha, F., Valera, A., Prudêncio, M.I. 2013. Luminescence and mineralogy of profiling samples from negative archaeological features. Mediterranean Archaeology and Archaeometry 13.3, 37-47. ISSN: 1108-9628.

Roberts, H.M., Duller, G.A.T. 2004. Standardised growth curves for optical dating of sediment using multiple grain aliquots. Radiat. Meas. 38, 241–252.

Roberts, R.G., Galbraith, R.F., Olley, J.M., Yoshida, H., Laslett, G.M., 1999. Optical dating of single and multiple grains of quartz from Jinmium rock shelter, northern Australia: Part II, Results and implications. Archaeometry 41, 365–395.

Sanderson, D.C.W., Chambers, D.A. 1985. An automated beta irradiator using a Sr-90 foil source. Ancient TL 3, 26-29.

Sharaf, J.M., Saleh, H. 2015. Gamma-ray energy buildup factor calculations and shielding effects of some Jordanian building structures. Radiat. Phys. Chem. 110, 87-95.

Singhvi, A.K., Stokes, S.C., Chauhan, N., Nagar, Y.C, Jaiswal, M.K. 2011. Changes in natural OSL sensitivity during single aliquot regeneration procedure and their implications for equivalent dose determination. Geochronometria 38, 231.241.

566 Soum, G., Mousselli, A., Arnal, F., Verdier, P. 1987. Etude de la transmission et de la
567 rêtrodiffusion d'électrons d'énergie 0,05 à 3MeV dans le domaine de la diffusion
568 multiple. Rev. Phys. Appl. 22, 1189-1209.
569 Spooner, N.A., Allsop, A. 2000. The spatial variation of dose-rate from 90Sr/90Y beta sources
570 for use in luminescence dating. Radiat. Meas. 32, 49-56.
571 Stokes, S. 1994. The Timing of OSL Sensitivity Changes in a Natural Quartz. Radiat. Meas. 23,
572 601-605.
573 Tabata, T., Andreo, P., Shinoda, K. 1999. Fractional energies of backscattered electrons and
574 photon yields by electrons. Radiat. Phys. Chem. 54, 11-18.
575 Tabata, T., Moskvin, V., Andreo, P., Lazurik, V., Rogov, Y. 2002. Extrapolated ranges of
576 electrons determined from transmission and projected-range straggling curves. Radiat.
577 Phys. Chem. 64, 161-167.
578 Thomsen, K.J. Murray, A.S., Bøtter-Jensen, L., 2005. Sources of variability in OSL dose
579 measurements using single grains of quartz. Radiat. Meas. 39, 47-61.
580 Toyoda, S., Rink, J.W., Schwarcz, H.P., Ikeya, M. 1996. Formation of E' Precursors in Quartz:
581 Applications to Dosimetry and Dating. Appl. Radiat. Isot. 47, 1393-1398.
582 Trubry, D.K. 1988. New Gamma-Ray Buildup Factor Data for Point Kernel Calculations: ANS-
583 6.4.3 Standard Reference Data. ORNL/RSIC 49, pp126.
584
585

5. Captions

Table 1. Samples, preparation and pretreatments

Table 2. Irradiators and sample presentation (Bortolot, pers comm; Lapp and Thomsen, 2010; Markey et al., 1997).

Table 3. Attenuation and buildup coefficients used in analytical calculations for air and quartz

Table 4. Luminescence readers and irradiation sequences. Cycle 1 irradiation times $t_{\beta 1}$ are listed in Table 5.

Table 5. Results of measurements, for each sample, grainsize and support

Table 6. Average 1σ % internal and external errors associated with single and multiple aliquot conversion coefficients (conversion coefficient = weighted mean of dose rates calculated using (2) or (3) for a given permutation of irradiator, support and grainsize). These uncertainty estimates do not include contributions from the absolute kerma calibration of the ^{60}Co irradiation, or the air kerma in air to dose in encapsulated quartz conversion (section 2.3).

Table 7. Conversion coefficients from weighted means of the best values for dose rate calculated using the multiple aliquot approach using $_{t\beta I/IT}$ (3), for each permutation of beta irradiator, grainsize, support, and signal integral. n is the number of samples measured per permutation (Table 1).

Table 8. Relative conversion factor for different types of support, as a function of grainsize and beta irradiator. Signal integral is Ch 11-30, 391-490.

Table 9. Ratios of measured / given beta exposure, and estimated / given gamma dose calculated using different conversion factors: “dose recovery”. The inverse of the recycling ratio from within the SAR sequence is included for comparison. Values are weighted means for a given sample, across the three different types of support (ALD, SSC, SSD), and hence also across the three different luminescence readers used for measurement (R1, R2, R3). % RMSD, $t_{\beta SAR}/t_{\beta}$ is the % root mean deviation from the $t_{\beta SAR}/t_{\beta}$ for that ratio.

Fig. 1. Flow diagram of operations and sub-samples in the calibration transfer procedure.

Fig. 2. Indicative spectrum of additional contribution to energy transported by Compton scattered electrons close to the wall-sample interface, resolved into forward- and sideways-scattered components. Electron scattering angle (φ), initial kinetic energy (T_{e0}), and probability distribution ($d\sigma_c/d\Omega$ vs. φ and hence T_{e0}) were obtained from the Compton scattering equations and Kline–Nishina formula (Krane, 1988 Ch7). Parallel (forward) and perpendicular scattering components were resolved as $T_{e0}\cos\varphi$ and $T_{e0}\sin\varphi$, these were used to calculate cdsa and hence extrapolated ranges (R_{cdsa}, $R_{ext,t}$; Berger et al., 2010; Tabata et al., 2002). $R_{ext,t}$ from the wall sample-interface is the abcissus, in units of cm into the sample (SiO_2 of bulk density ρ = 1.6 gcm^{-2}). A degraded spectrum was obtained by integrating $f(T_{e0max} - T_e) = d\sigma_c/d\Omega$ between 0 and ($T_{e0max} - T_{e0}$), then integrated again as a function of T_{e0} resolved according to its directional components. These were normalised to the integral of the complete undegraded spectrum and multiplied by $((\rho_W/\rho_S)-1)/2$, to obtain fraction of extra transported energy in the sample as a function of distance from the wall/sample interface. The sum of the integrals of each directional component, divided by the sample half thickness (0.4 cm), indicates an overall addition of 0.48% to energy deposition in the sample.

Fig. 3. Absorbed dose and collisional kerma vs. depth along the ^{60}Co source - sample axis, with (D_S, K_{ColS}) and without (K_{ColA}) the sample present, calculated in EGSnrc using an end-on cylindrical approximation of the sample geometry (see text for details).

Fig. 4. Backscatter energy coefficients for electrons of initial kinetic energy (T_{e0}) between 0 and 1.6 MeV, normally incident on 0.25 mm Fe (SSC), 0.5 mm Fe (SSD), and 0.5 mm Al (ALD). Inset are shown SSC and SSD values normalised to ALD. Backscatter energy coefficients for semi-infinite media were calculated from Tabata et al. (1999), and the effect of thickness on number coefficient calculated from Soum et al. (1987).

Fig. 5. Standardised dose response, and predose sensitization, of SAR-OSL. Values are weighted means for each {sample; support/reader} permutation measured (n ≈ 48): black symbols = SSC/R1, dark grey symbols = ALD/R2, light grey symbols = SSD/R3.

Tables

Table 1. double column table

Sample	Source	Grain-size (μm)	Pretreatment	Irradiation - Measurement (days)
A12/175	Miocene arenite	90-160	700 °C / 1 hr; 10 kGy; 500 °C / 0 min	1
A9/203	Holocene heated colluvium	160-250	350 °C / 0 min	20
A9/202	Holocene colluvial soil	100-160	Bleach, daylight behind window	13
A9/291	Holocene palaeosol	90-160	Bleach, daylight behind window	6
A6/485	Pliocene coastal dune sand	160-250	Bleach, daylight behind window	3
A10/161	Late Holocene coastal dune sand	160-250	Bleach, daylight behind window	10
A7/318	Recent coastal dune sand	160-250	Bleach, daylight behind window	2

664 Table 2. double column table

665

Irradiator	Label Model	^{60}Co AECL Eldorado 6	R1 Risø DA-15	R2 Risø DA-20	R3 Risø DA-20	Db Daybreak 801E
Source	Type Model	^{60}Co	^{90}Sr/^{90}Y Amersham	^{90}Sr/^{90}Y Eckert & Ziegler	^{90}Sr/^{90}Y Eckert & Ziegler	^{90}Sr/^{90}Y AEA Technology
	Nominal Activity	92.5 TBq, Co(Ni) in steel capsule	1.48 GBq, 2000 in 12 mm diameter Ag foil	1.48 GBq, 2007 1 ceramic bead melted into 1 cm diameter steel cup	1.48 GBq, 2009 4 ceramic beads deposited in 1 cm diameter steel cup	7.4 GBq, 2002 1 ceramic bead, 5 mm diameter, on steel
Sample		Bulk powder, 8×8×16 mm, $\rho \approx 1.6$ gcm^{-3}	ca. 5 mm diameter monolayer, central on:			
Container / Support		Fused silica, walls 3.7±0.05 mm $\rho = 2.2$ gcm^{-3}	stainless steel cups (SSC), 0.25 mm thickness; aluminium disks (ALD), 0.5 mm thickness; stainless steel disks (SSD), 0.5 mm thickness			
Substrate		Air	N_2			Aluminium
Source - sample	(mm)	800	7 disk; 8 cup			15 disk; 15.5 cup

666

667

Table 3. single column table

		Air	SiO_2
μ_{tot}	cm^2g^{-1}	0.05687	0.05693
μ_{nc}	cm^2g^{-1}	0.05684	0.05686
μ_c	cm^2g^{-1}	0.05682	0.05682
μ_{en}	cm^2g^{-1}	0.02666	0.02661
a		2.0205	1.9598
b		1.3465	1.3075
c		-0.0715	-0.0626
ξ		14.295	14.958
d		0.0288	0.0226

Table 4. single column table

Reader Support Cycle	R1 SSC t_B (s)	R2 ALD	R3 SSD
1	-	-	-
2	68	63	36
3	0	0	0
4	17	16	9
5	34	32	18
6	136	126	72
7	272	252	144
8	0	0	0
9	68	63	36
10 (IR)	68	63	36
T	14	13	7

Table 5. double column table

Sample	Irradiation			Measurement															
Grainsize				SSC, R1					ALD, R2					SSD, R3					
(μm)				n I	I_S	$t_{\theta SAR}$	RR	Z2	n I	I_S	$t_{\theta SAR}$	RR	Z2	n I	I_S	$t_{\theta SAR}$	RR	Z2
Date				(cts)	(sβ)	(sβ)		(sβ)	(cts)	(sβ)	(sβ)		(sβ)	(cts)	(sβ)	(sβ)		(sβ)
A12/175	R1	68	(sβ)	8 13671	55	66	1.05	0.6	8 29244	55	62	1.01	0.6	8 64628	35	40	1.03	0.3
90-160	R2	51	(sβ)	8 13663	49	58	1.06	0.7	8 5839	53	60	1.00	0.6	8 56189	34	38	1.03	0.4
18-04-13	R3	42	(sβ)	8 13744	49	58	1.05	0.7	7 32875	54	61	1.01	0.6	8 61988	31	35	1.03	0.4
	Db	30	(sβ)	8 13028	53	63	1.05	0.7	6 25215	47	52	1.02	0.6	8 54380	29	32	1.04	0.4
	^{60}Co	4.62	(Gy)	8 11688	50	58	1.08	0.6	8 28824	43	46	1.03	0.6	8 51873	29	32	1.03	0.3
	Bl	0		8 17	0.1	-0.4	1.12	0.8	8 16	0.0	-0.3	1.06	0.6	8 11	0.0	-0.2	1.06	0.4
A9/203	R1	68	(sβ)	8 8634	55	72	0.91	0.2	7 37612	*34*				8 49463	40	46	0.97	0.1
160 - 250	R2	51	(sβ)	8 9580	51	66	0.87	0.2	8 28030	*33*				8 55298	36	42	0.97	0.1
26-06-13	R3	42	(sβ)	8 7782	51	65	0.87	0.2	6 23845	*33*				8 42232	33	37	0.97	0.1
	Db	30	(sβ)	8 9499	55	72	0.93	0.2	8 24873	*32*				8 41074	31	35	0.96	0.1
	^{60}Co	4.62	(Gy)	8 12299	57	73	0.92	0.2	6 31145	*25*				8 36872	33	37	0.97	0.1
	Bl	0		7 4	0.0	-0.1	0.88	0.2	8 4	*0.0*				8 -2	0.0	-0.1	0.97	0.1
A9/202	R1	68	(sβ)	8 783	43	56	1.01	1.5	8 16892	53	62	1.00	1.0	8 29996	34	40	1.01	0.6
100-160	R2	51	(sβ)	8 1038	42	55	0.98	1.6	7 12298	50	58	1.00	1.1	7 23430	32	37	1.00	0.7
02-08-13	R3	42	(sβ)	8 1069	41	53	1.00	1.4	8 8871	54	62	0.99	1.1	8 23988	30	34	0.99	0.6
	Db	30	(sβ)	8 1145	46	60	0.97	1.6	6 8741	45	51	0.98	1.0	8 25824	27	31	1.01	0.7
	^{60}Co	4.62	(Gy)	8 1079	45	58	0.93	1.2	8 14999	41	46	0.97	1.2	8 21348	27	31	0.98	0.7
	Bl	0		8 12	0.3	-0.4	0.93	1.3	7 67	0.3	-0.4	0.97	1.1	8 100	0.2	-0.2	0.99	0.6
A9/291	R1	78	(sβ)	7 626	53	69	1.05	0.5	8 6689	45	52	0.99	0.5	8 3326	29	32	0.98	0.3
90-160	R2	61	(sβ)	8 561	53	68	1.06	0.5	8 16281	46	53	0.98	0.6	8 5136	30	35	0.98	0.3
12-05-14	R3	51	(sβ)	8 805	53	66	1.02	0.5	8 6410	44	50	0.99	0.6	8 5780	29	32	1.00	0.3
	Db	33	(sβ)	8 421	50	63	0.97	0.7	7 13288	42	47	1.00	0.5	8 3692	29	32	1.01	0.3
	^{60}Co	4.62	(Gy)	8 631	45	56	0.98	0.6	8 20309	40	45	1.00	0.5	8 5602	27	29	1.01	0.3
	Bl	0		8 4	0.4	0.0	1.01	0.7	8 143	0.3	0.0	1.00	0.5	7 24	0.2	0.0	1.02	0.3
A6/485	R1	78	(sβ)	8 30657	49	62	1.03	1.2	8 2865	39	46	1.02	1.0	8 68892	27	31	1.01	0.8
160 - 250	R2	61	(sβ)	8 40174	48	60	1.03	1.1	8 2388	43	48	0.99	0.7	8 68370	26	31	1.01	1.0
04-07-14	R3	51	(sβ)	7 36360	45	56	1.03	1.0	8 3104	40	45	1.01	1.1	8 77307	27	31	1.01	0.7
	Db	33	(sβ)	8 34433	47	58	1.03	1.1	8 2042	39	43	1.02	0.8	8 84386	26	30	1.01	0.8
	^{60}Co	4.62	(Gy)	8 21961	45	55	1.02	1.6	8 3958	37	40	0.98	0.8	8 47990	25	30	1.01	1.1
	Bl	0		8 1279	1.7	0.9	1.09	1.4	8 62	1.0	0.5	1.03	0.8	8 1467	0.6	0.1	1.01	0.8
A10/161	R1	78	(sβ)	8 3333	46	63	1.01	1.4	6 882	43	50	0.99	1.6	8 16493	24	34	1.03	1.1
160 - 250	R2	61	(sβ)	8 5913	48	66	0.99	2.4	8 841	43	48	0.98	0.9	8 18997	27	34	1.00	1.0
31-10-14	R3	51	(sβ)	8 5566	46	63	1.02	1.3	6 2284	41	46	1.00	1.2	8 23337	24	30	0.97	1.1
	Db	33	(sβ)	8 6332	48	64	1.00	1.3	7 1163	44	49	1.02	1.0	7 16436	27	34	0.96	1.0
	^{60}Co	4.62	(Gy)	8 3060	46	64	1.01	1.5	5 646	32	37	1.01	1.8	8 15572	26	32	0.98	1.0
	Bl	0		8 375	2.5	1.6	1.01	1.7	8 45	0.9	0.3	1.02	0.8	7 577	0.9	0.0	0.95	1.2
A7/318	R1	78	(sβ)	8 17547	17	60	1.23	4.5	8 3153	21	50	1.09	2.9	8 28570	17	35	1.14	1.1
160 - 250	R2	61	(sβ)	8 17597	18	59	1.22	4.4	8 701	22	54	1.09	3.2	8 81845	15	36	1.07	1.3
05-09-14	R3	51	(sβ)	8 13164	17	58	1.22	4.0	8 2767	20	50	1.17	3.2	8 107844	16	33	1.11	1.3
	Db	33	(sβ)	7 10952	17	63	1.16	4.0	8 2885	22	50	1.08	2.7	8 74777	18	36	1.17	1.2
	^{60}Co	4.62	(Gy)	8 17648	17	62	1.28	4.9	8 2866	19	47	1.11	3.6	8 64049	16	35	1.04	1.3
	Bl	0		8 303	0.4	0.5	1.24	4.5	7 30	0.2	-1.3	1.06	3.4	8 609	0.1	-0.6	1.05	1.6

Numbers in italics: break in run, I normalised to subsequent regenerative dose response

687 Table 6. single column table

688

	C_{MA}		C_{SA}	
OSL signal integrals	int	ext	int	ext
Ch 11-30, 391-490	1.3	1.5	0.9	3.8
Ch 11-12, 13-14	1.3	1.9	1.2	3.6

689

690

691 Table 7. single column table

692

C		OSL signal integrals			
Multiple		11-30;391-490		11-12;13-14	
Aliquot		C	±*	C	±*
		($mGy^{60}Co\ s^{-1}$)			
Stainless Steel Cup	R1	73.6	2.0	76.4	3.2
90/100-160 µm	R2	91.5	1.3	94.6	3.0
n = 3	R3	110.2	1.5	111.9	3.7
	Db	166.1	2.0	170.2	6.5
Stainless Steel Cup	R1	68.3	1.1	67.7	1.1
160 - 250 µm	R2	86.3	1.4	85.4	1.5
n = 4	R3	100.3	1.6	100.4	1.6
	Db	155.6	2.5	154.8	2.6
Aluminium Disk	R1	71.4	0.9	72.5	1.2
90/100-160 µm	R2	93.0	0.9	93.8	0.8
n = 3	R3	113.7	1.5	114.5	2.1
	Db	136.8	1.4	137.0	1.8
Aluminium Disk	R1	75.5	3.1	75.3	2.6
160 - 250 µm	R2	97.2	1.8	98.2	2.6
n = 4	R3	114.9	3.6	115.0	3.5
	Db	145	10	147.3	11
Stainless Steel Disk	R1	91.6	1.3	92.6	1.1
90/100-160 µm	R2	116.0	1.1	115.5	1.8
n = 3	R3	143.4	1.7	141.5	2.4
	Db	170.3	3.1	167.2	3.3
Stainless Steel Disk	R1	89.5	3.2	89.7	1.0
160 - 250 µm	R2	110.0	1.1	110.9	1.0
n = 4	R3	131.0	5.3	131.3	4.7
	Db	164.2	1.9	164.9	3.8

* Max{s, σ} combined with kerma and kerma-to-dose

693

694

695 Table 8. single column table

696

Grainsize	Irradiator	C/C_{ALD}			
		SSC		SSD	
90/100-160 μm					
	R1	1.03	0.03	1.28	0.02
	R2	0.98	0.02	1.25	0.02
	R3	0.97	0.02	1.26	0.02
	Db	1.21	0.02	1.24	0.02
160 - 250 μm					
	R1	0.90	0.04	1.19	0.06
	R2	0.89	0.02	1.13	0.02
	R3	0.87	0.03	1.14	0.05
	Db	1.08	0.06	1.14	0.06

697

698

699 Table 9. double column table
700

		Ch 11-30, 391-490					Ch 11-12, 13-14				
		Beta		Gamma			Beta		Gamma		
			Meas/Given	Estimated/Given				Meas/Given	Estimated/Given		
Sample	Grainsize	1/RR	$t_{\beta SAR}$	$\dot{D}_{\beta MA}$	C_{SA}	C_{MA}	1/RR	$t_{\beta SAR}$	$\dot{D}_{\beta MA}$	C_{SA}	C_{MA}
A12/175	90-160	0.98	0.96	0.94	1.01	0.92	0.99	0.96	0.95	1.01	0.93
A9/203	160-250	1.04	1.05	1.14	1.09	1.03	1.04	1.05	1.13	1.11	1.05
A9/202	100-160	1.00	0.93	0.93	0.99	0.91	1.02	0.94	0.93	0.99	0.90
A9/291	90-160	1.01	0.87	0.87	0.94	0.85	1.02	0.89	0.90	0.96	0.88
A6/485	160-250	0.99	0.80	0.82	0.90	0.78	0.99	0.79	0.86	0.89	0.76
A10/161	160-250	1.02	0.79	0.89	0.91	0.83	1.02	0.81	0.94	0.93	0.85
A7/318	160-250	0.85	0.83	0.97	1.03	0.88	0.93	0.84	0.95	0.99	0.86
% RMSD, $t_{\beta SAR}/t_{\beta}$		12.6	0.0	7	10	3.2	13	0.0	8	9	2.8
Mean		0.98	0.89	0.94	0.98	0.89	1.00	0.90	0.95	0.98	0.89
Std. Dev.		0.06	0.09	0.10	0.07	0.08	0.04	0.09	0.09	0.07	0.09

701
702

703 Figures

704

705

706 Fig. 1. Double column figure

707

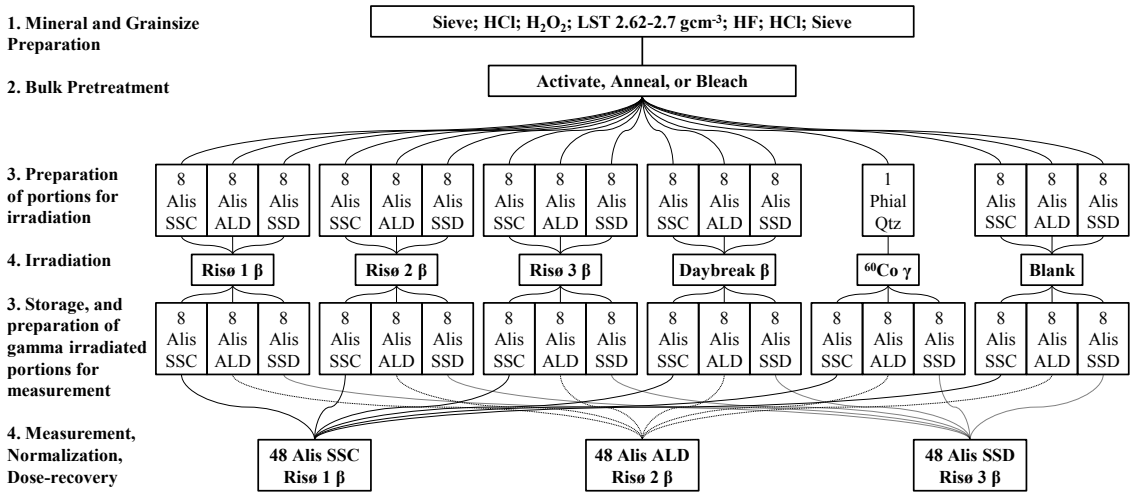

708

709

710

711

712

713

714 Fig. 2. Single column figure

715

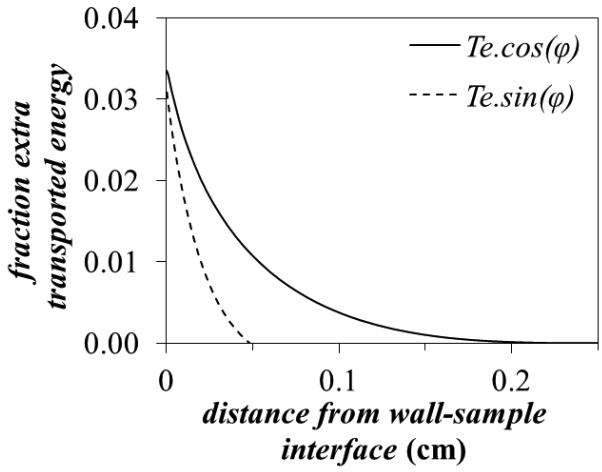

716

717

718

719 Fig. 3. Single column figure

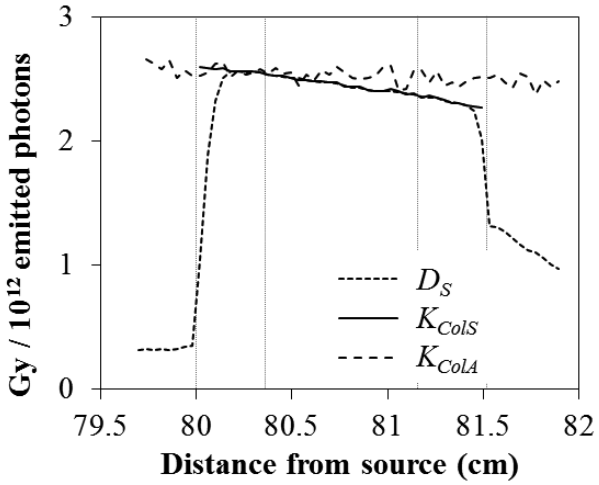

720

721

722 Fig. 4. Single column figure

723

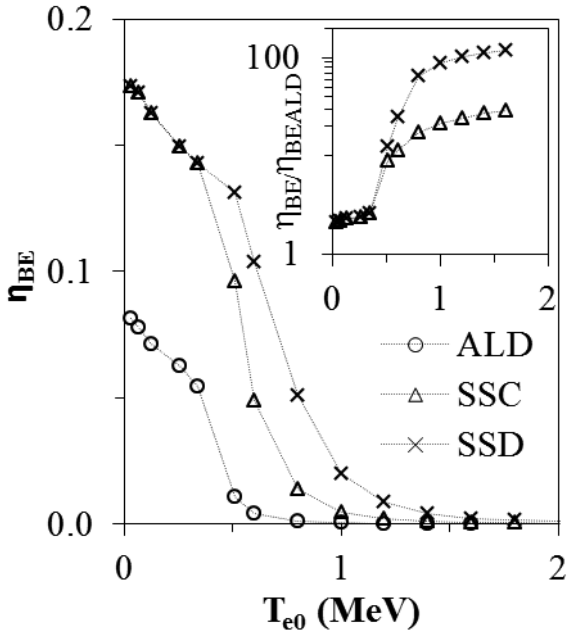

724

725

726

727 Fig. 5. Single column figure

728

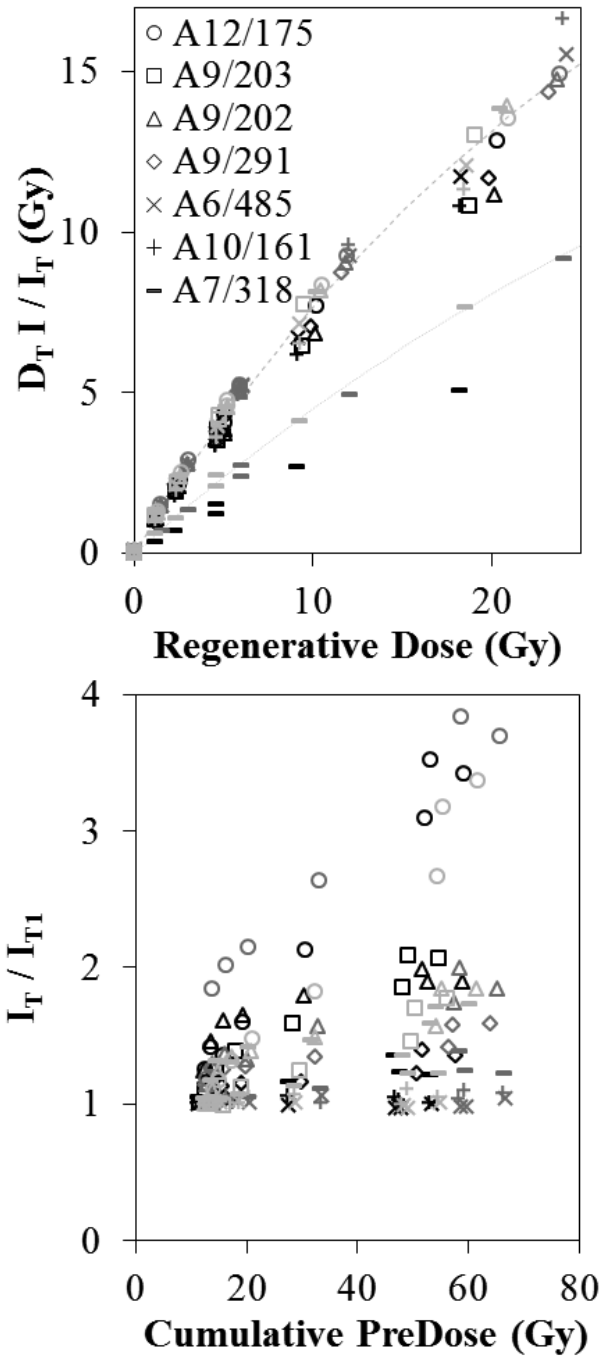

729

730

731